Asian Journal of Chemistry; Vol. 32, No. 2 (2020), 420-426

ASIAN JOURNAL OF CHEMISTRY

https://doi.org/10.14233/ajchem.2020.22448

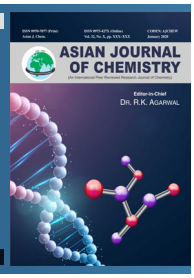

Synthesis and Structural, Optical, Photoluminescence and Electronic Structure Studies of $SrAl_2O_4$ Phosphor

SUJATA TONGBRAM[1,2], S. DORENDRAJIT SINGH[3], BINITA TONGBRAM[4] and B. INDRAJIT SHARMA[1,*]

[1]Department of Physics, Assam University, Silchar-788011, India
[2]Department of Physics, N.I.T. Manipur, Imphal-795001, India
[3]Department of Physics, Manipur University, Imphal-795003, India
[4]Department of Electrical Engineering, Indian Institute of Technology Bombay, Mumbai-400076, India

*Corresponding author: E-mail: indraofficial@rediffmail.com

Received: 14 September 2019; *Accepted*: 31 October 2019; *Published online*: 30 December 2019; AJC-19737

In this work, pure $SrAl_2O_4$ phosphor is synthesized using precipitation method annealed at 1000 ºC and characterized by XRD, FTIR, UV-visible, Raman, SEM, EDX, TEM, SAED and photoluminescence spectroscopy. The XRD pattern reveals the unit cell structure of $SrAl_2O_4$ as monoclinic. The SEM and TEM images show a non-uniform shape with agglomeration, and its size varies from 10 to 80 nm. The SAED pattern confirms polycrystalline and single crystal in the different selected area with different magnification. Photoluminescence emission shows a peak at 467 nm (blue) when excited at 272 nm wavelength. The electronic structure calculation with the density functional theory (DFT) shows a band gap of 4.4 eV, which is nearly equal to 4.46 eV obtained from the experiment optical absorption spectrum. The findings would be beneficial for furthermore investigations on doping in the pure $SrAl_2O_4$ phosphor to enhance its high luminescent intensity and long-lasting for a future technological purpose.

Keywords: Strontium aluminates, Precipitation method, Electronic structure, DFT.

INTRODUCTION

Lanthanide-doped strontium aluminates phosphor are one of the promising materials possessing excellent properties of high luminescent intensity, long-lasting time, chemical stability, emitting suitable colour and eco-friendliness. These excellent properties direct to various applications in many fields, such as traffic, emergency signs, the dial plates of the night watch and interior decoration as well as in the textile industry [1,2]. However, the luminescence emission of doped phosphor is strongly dependent on the host lattice and emits from the ultra-violet to red region. So, there is a need to understand and investigate pure host, strontium aluminates ($SrAl_2O_4$) phosphor lattice thoroughly.

This paper reports the detailed synthesis and characterization of pure $SrAl_2O_4$ phosphor, its band gap calculation using density functional theory (DFT) and compare with the experimental value obtained from the UV-visible spectrum. Various chemical synthesis techniques such as solid-state reaction, sol-gel, reverse micro-emulsion, combustion method and precipitation method are generally used to prepare the phosphor. Among them, the precipitation method is the commonly used method since it is safe; no adverse chemical reaction takes place and less time-energy consumed. The phase formation and the particles size are investigated using XRD, SEM and TEM. Also, FTIR and Raman studies are carried out for determining its functional groups. The findings would be useful in selecting appropriate elements such as lanthanide for doping in pure $SrAl_2O_4$ phosphor to increase its high luminescent intensity and long-lasting time for the future technological purpose.

EXPERIMENTAL

The materials used are aluminium nitrate [$Al(NO_3)_3{\cdot}9H_2O$], strontium nitrate [$Sr(NO_3)_2$] and ammonium carbonate [$(NH_4)_2CO_3$]. All the materials are of analytical grade, so no further purification required.

Synthesis of pure $SrAl_2O_4$: Pure $SrAl_2O_4$ is prepared by using the precipitation method [3,4]. In this method, 1 M of $Sr(NO_3)_2$ and 2 M of $Al(NO_3)_3{\cdot}9H_2O$ were dissolved together

in distilled water using magnetic stirrer for 1 h. Using $(NH_4)_2CO_3$ as precipitant, the solution is maintained at pH value 8-9 and kept overnight. The resultant solution is centrifuged and washed several times using distilled water and acetone. The product material is dried in an oven at 100 ºC for 48 h. Finally, annealing is done at 1000 ºC for 4 h in the ambient atmosphere. Thus, obtained sample is white in powder form.

Characterization: The structural properties are studied by collecting the XRD patterns of the samples using Panalytical X′Pert Pro diffractometer with CuK_α at $\lambda = 0.15405$ nm. From the XRD pattern, the grain size is calculated using the Debye-Scherrer Formula. The morphology and particle size of powder samples are analyzed using scanning electron microscopy (SEM) model JSM-7600F with accelerating voltage 0.1 kV to 30 kV and transmission electron microscopy (TEM) model Tecnai G2 F30 with 300 kV. The chemical composition is determined by energy-dispersive X-ray spectroscopy (EDX). The FTIR measurement is carried out using Perkin-Elmer FTIR spectrometer and optical properties are studied using Perkin-Elmer Lambda-35 UV-Vis spectrometer. For the photoluminescence study, the samples are excited at 272 nm; the spectra are measured using F-7000 FL spectrophotometer in the range of 400-700 nm. The Raman spectroscopy is also investigated using Horiba HR 800 model with excitation wavelength 514.5 nm.

RESULTS AND DISCUSSION

XRD analysis: The analysis of XRD data is usually based on the relative peak intensities. Based on XRD data, it is used to identify the crystalline phases, to determine phase composition, and to estimate the particle size of the materials. XRD is also used to identify the presence of any impurity phases from the host material. Fig. 1a shows the XRD pattern of $SrAl_2O_4$ phosphor without heat treatment. The peaks in the XRD pattern do not match with the JCPDS (Joint Committee on powder diffraction standard data), and so heat treatment is given to the $SrAl_2O_4$ phosphor sample at 1000 ºC. XRD pattern of $SrAl_2O_4$ phosphor annealed at 1000 ºC for 4 h is shown in Fig. 1b. The XRD pattern revealed a monoclinic structure with space group $P2_1$ matching well with JCPDS data (file no. 01-074-0794). The crystallite size is calcu-lated using the Scherrer′s formula [3,5,6]:

$$D = \frac{k\lambda}{\beta \cos(\theta)} \quad (1)$$

where D is the crystallite size, β is the full width at half maximum height of diffraction peak, λ is the X-ray wavelength, θ is the Bragg′s angle, k = 0.9 is Scherrer′s constant. Thus, the crystallite size is calculated for the maximum diffraction peak (0 3 1) that corresponds to 2θ = 35.34º and is found to be 25.73 nm. The lattice parameter and the unit cell volume were calculated; both the experimental and the standard values were nearly equal (Tables 1 and 2), which indicate the formation of $SrAl_2O_4$ phosphor monoclinic structure.

FTIR analysis: Fig. 2 shows the FTIR spectrum of $SrAl_2O_4$ phosphor. The bands between 1000 and 350 cm^{-1} correspond to the IR active vibration modes and associated with changes in the dipole moment. The band at 1485.43 cm^{-1} is attributed

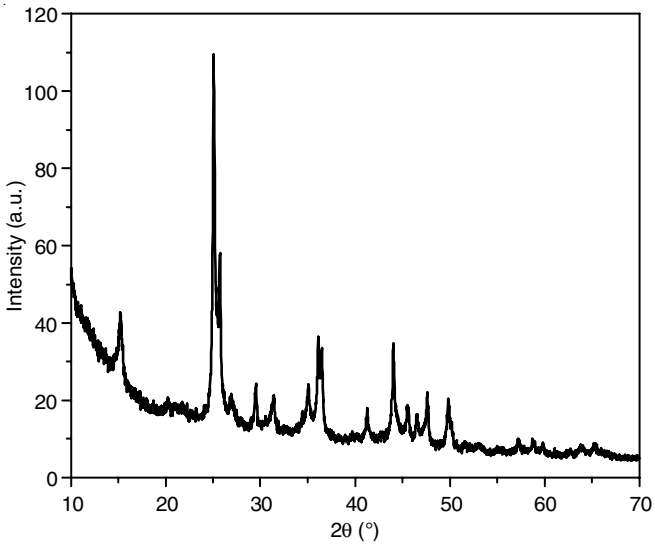

Fig. 1(a). XRD pattern of $SrAl_2O_4$ phosphor with no heat treatment

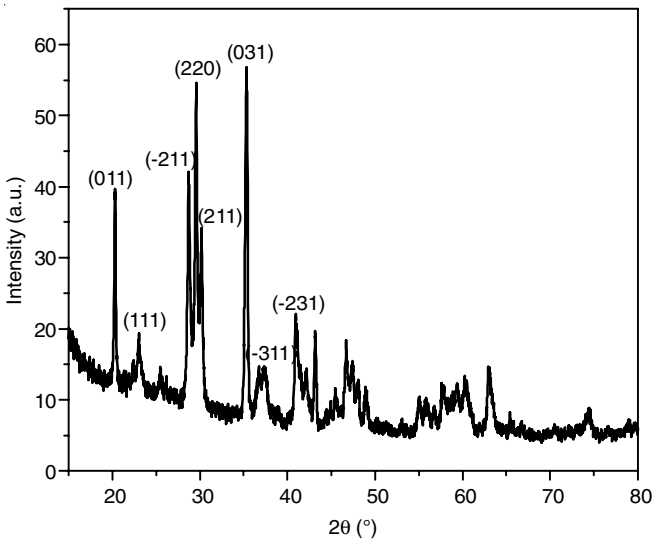

Fig. 1(b). XRD pattern of $SrAl_2O_4$ phosphor with heat treatment at 1000 °C

TABLE-1
EXPERIMENTAL RESULT FOR THE UNIT CELL LATTICE PARAMETER OF $SrAl_2O_4$

$SrAl_2O_4$ phosphor annealed at 1000 °C	JCPDS data	Experimental (this work)
a (Å)	8.447	8.439
b (Å)	8.816	8.748
c (Å)	5.163	5.112
β (°)	93.42	93.70
Volume (10^6 pm^3)	383.800	376.580

TABLE-2
CRYSTALLOGRAPHIC PARAMETERS OF $SrAl_2O_4$ PHOSPHOR

(h k l) value	d values (Å) (JCPDS data)	2θ (JCPDS data)	d values (Å) (this work)	2θ (this work)
0 1 1	4.449	19.940	4.375	20.285
1 1 1	3.854	23.059	3.854	23.058
-2 1 1	3.142	28.381	3.109	28.690
2 2 0	3.047	29.290	3.016	29.600
2 1 1	2.984	29.914	2.958	30.196
0 3 1	2.553	35.125	2.538	35.338
-3 1 1	2.434	36.908	2.447	36.701
-2 3 1	2.213	40.742	2.202	40.948

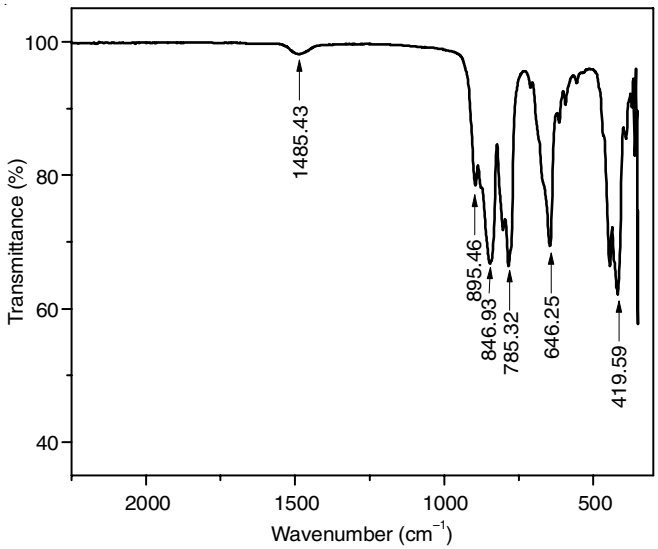

Fig. 2. FTIR spectrum of $SrAl_2O_4$ phosphor

to the C-O vibration. The two bands positioned at 785.32 and 895.46 cm^{-1} originate from the aluminates groups (AlO_4). The band located at 646.25 and 846.93 cm^{-1} attributes to Sr-O vibrations and the band at 419.59 cm^{-1} corresponds to O-Al-O vibrations [7].

UV-visible analysis: Fig. 3a shows the optical absorption spectrum of pure $SrAl_2O_4$ phosphor. The spectrum shows weak broad band between 210 and 400 nm. These bands may be attributed to structural defects in $SrAl_2O_4$ phosphor. Absorption bands above 400 nm are not observed due to the wideness of band gap [7,8]. In this work, the absorption is observed at 227 and 264 nm. The optical energy band gap of $SrAl_2O_4$ phosphor is calculated using the Tauc relation [8,9]:

$$(\alpha h\nu)^2 = k^2(h\nu - E_g) \quad (2)$$

where α is the absorption coefficient, $h\nu$ is the photon energy, k is a constant depends on the type of transition, E_g is the band gap. Thus, the band gap is determined by plotting $(\alpha h\nu)^2$ *versus* $h\nu$ in the high absorption range and the linear region extrapolates to $(\alpha h\nu)^2$ as shown in Fig. 3b. The point where the extrapolation of linear region intersects the $h\nu$ axis is taken as the band gap and its estimated value is found to be 4.46 eV.

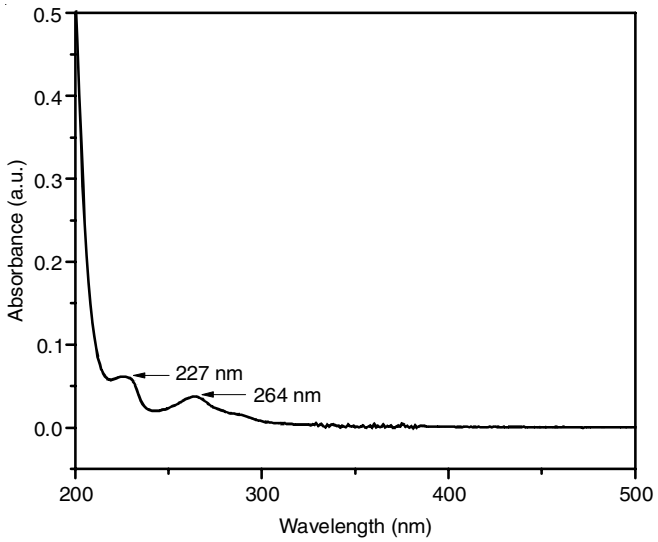

Fig. 3(a). Absorption spectrum of $SrAl_2O_4$ phosphor

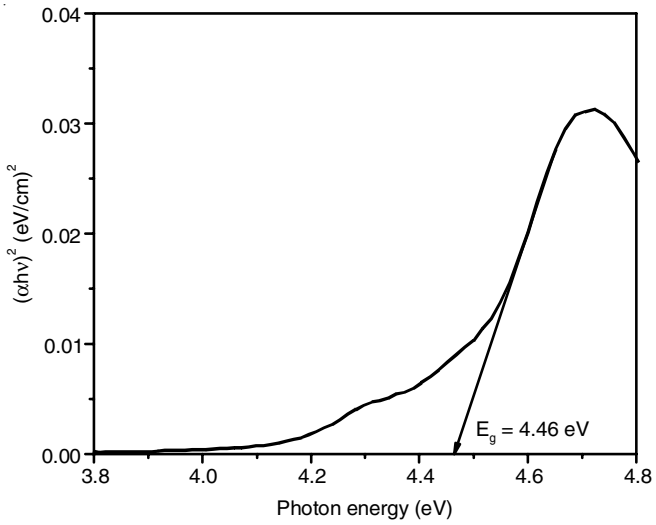

Fig. 3(b). Tauc plot: $(\alpha h\nu)^2$ *versus* $h\nu$ of $SrAl_2O_4$ phosphor

Raman analysis: Fig. 4 shows the Raman spectrum of $SrAl_2O_4$ phosphor, and the modes at a frequency higher than 600 cm^{-1} attributes to Al-O stretching vibrations and the narrow low-frequency peaks below 250 cm^{-1} to tetrahedral vibrations or tilts (O-O-O angle between linked tetrahedral). The peak at 464 cm^{-1} contributes to the bending of O-Al-O bonds in corner-sharing tetrahedral, indicating that the polymorphs are present close to the monoclinic structure [5,10].

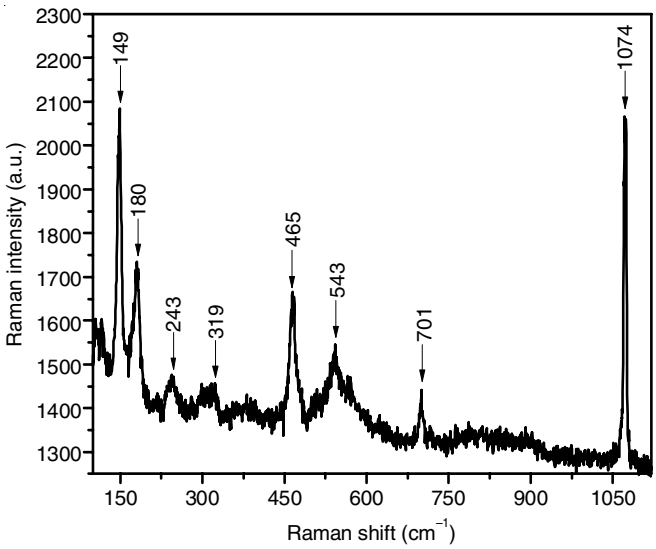

Fig. 4. Raman spectrum of $SrAl_2O_4$ phosphor

SEM analysis: Fig. 5a-b show the SEM micrographs of $SrAl_2O_4$ phosphor at two different magnification 50K and 75K, respectively to investigate the surface morphology and its average crystallite size. The phosphors are in the form of nanoparticles, which are easily aggregate together. The SEM images show irregular shape with sizes varying from 10 to 80 nm, illustrating the nanoscaled phosphors. The wide particle size distribution as well as the irregular shape of particles, is probably due to non-uniform distribution of temperature. However, looking closer observes some near-spherical particles. The morphology also shows the plate-like structure, which is an advantage in the light out-coupling strategies for designing devices.

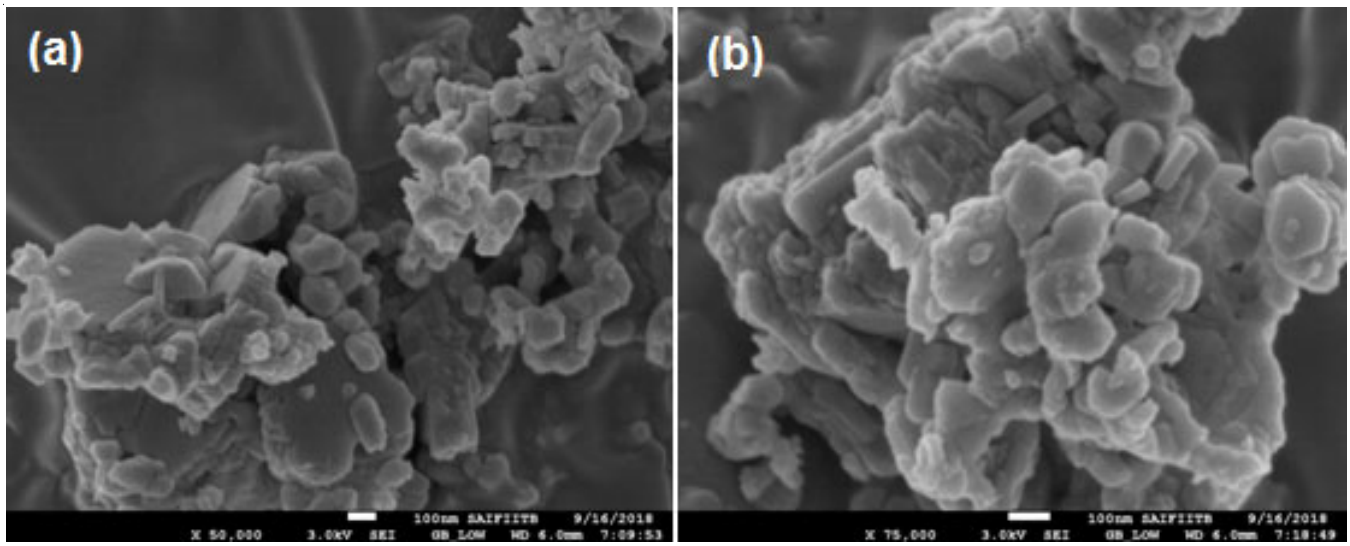

Fig. 5. SEM micrograph of $SrAl_2O_4$ phosphor taken at (a) 50 K and (b) 75 K magnification

EDX analysis: The elemental compositions of phosphor were determined by EDX. An EDX spectrum displays peaks corresponding to the energy level for which the most X-ray received. Fig. 6a shows the selected area image of $SrAl_2O_4$ phosphor used to conduct the elemental mapping of phosphor and Fig. 6b gives the EDX spectrum that corresponds to the presence of Sr, Al and O in the sample. The maximum intensity corresponds to element aluminium. Traces of other elements are not found that indicates the formation of perfect $SrAl_2O_4$ phosphor. The atomic percentage of aluminium is approximately equal to 2 times of strontium (inset table in Fig. 6b) that shows the formation of sample nearly equal to their mole concentration ratio as taken while preparing of the phosphor.

TEM analysis: Fig.7a-b represents TEM images of $SrAl_2O_4$ phosphor at 200 nm and 0.5 µm magnification, respectively. The phosphor shows a nearly spherical shape without much agglomeration and the particles size is in the range of 5-112 nm, which are calculated using ImageJ software. Fig. 8a-b shows the high-resolution transmission electron microscopy $SrAl_2O_4$ phosphor at 5 nm, and 10 nm magnification and the calculated d-spacing values at these magnifications are 3.0400 and 3.0577 Å, respectively which are reasonably comparable with the standard value, 3.04677 Å. The SAED images were also shown as an inset in Fig. 8, which supports the crystalline phases.

Photoluminescence analysis: The excitation and emission spectra of $SrAl_2O_4$ phosphor at room temperature are shown in Fig. 9a-b, which shows a blue shift in the emission spectrum that corresponds to the nano-range grain size of the strontium aluminates phosphor. Fig. 9a shows a broad peak at 272 nm indicates the appropriate wavelength for excitation. In the emission spectrum, as shown in Fig.9(b), there are a broadband near 445 nm and a sharp peak at 467 nm. The sharp peak represents the blue emis-sion, which may be due to an oxygen defect in $SrAl_2O_4$ phos-phor and the broadband is not able to consistent with the band-to-band emission [10]. Also, the emission does not arise from the activator or co-activator ions indicated that defect centers act as trap levels in bringing

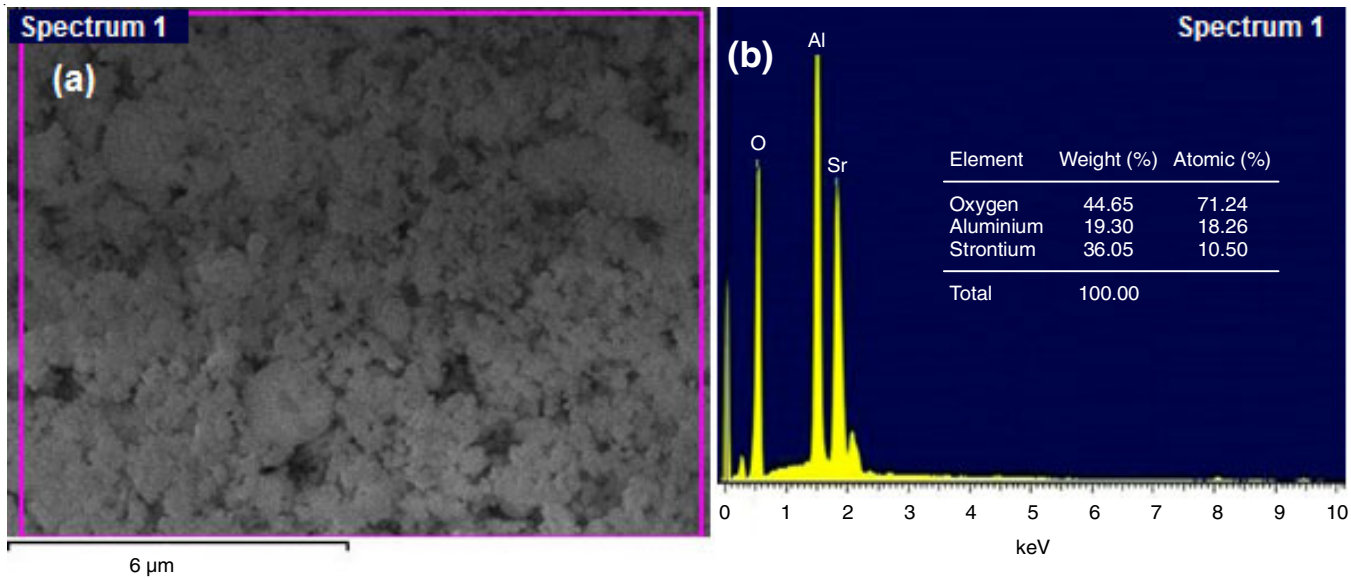

Fig. 6. (a) Selected area image and (b) EDX spectrum of $SrAl_2O_4$ phosphor

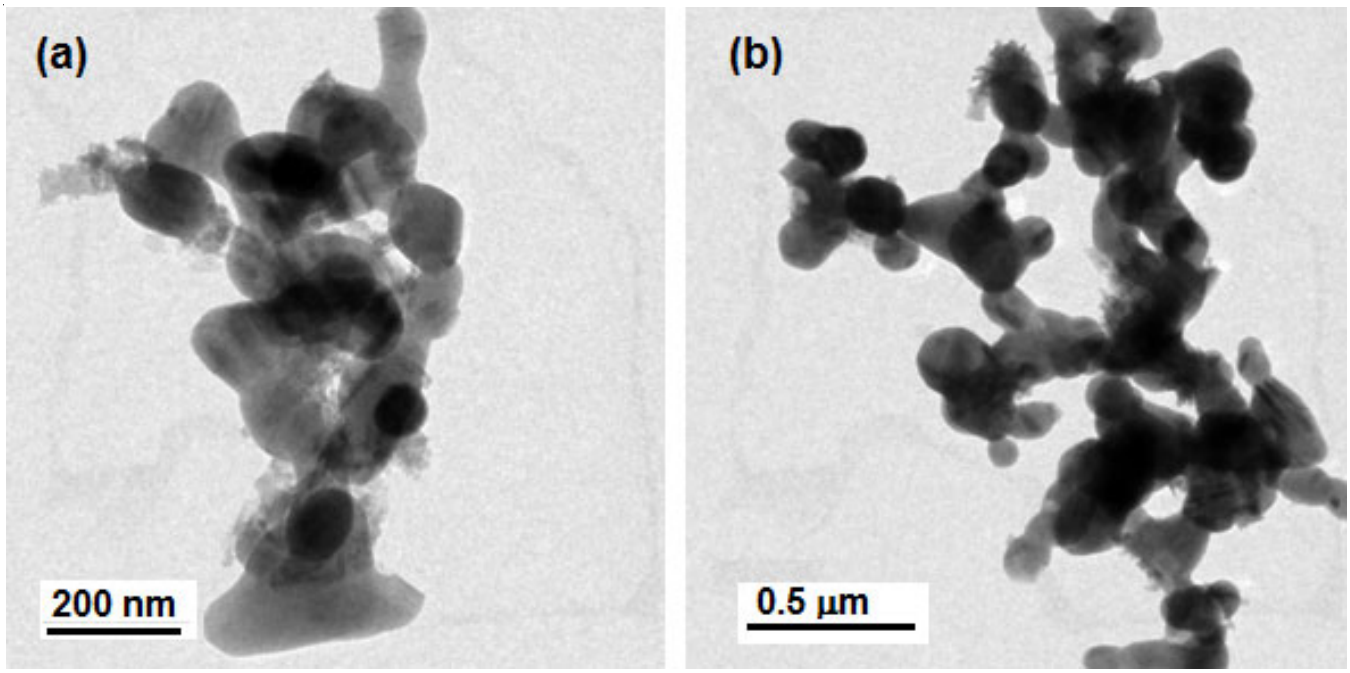

Fig. 7. TEM images at (a) 200 nm and (b) 0.5 µm magnification of $SrAl_2O_4$ phosphor

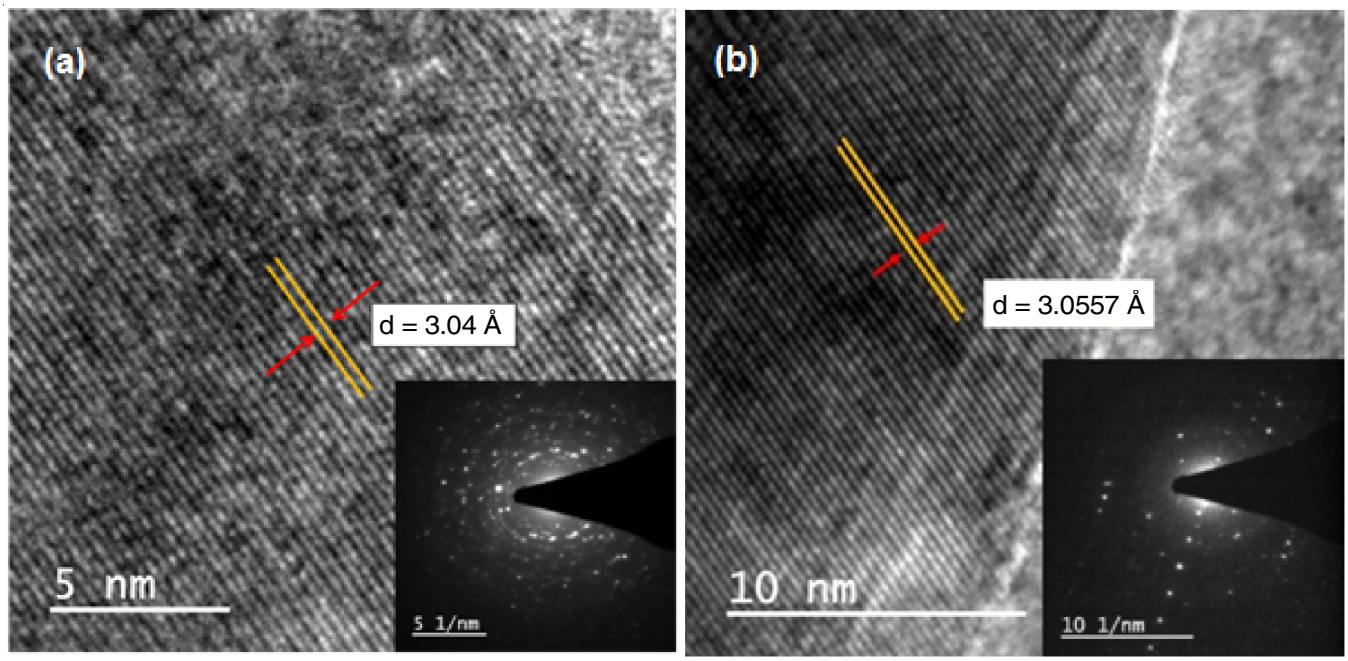

Fig. 8. HRTEM images at (a) 5 nm and (b) 10 nm magnification with corresponding SAED image (inset) of $SrAl_2O_4$

out the emissions [11]. The defects responsible for bands at 445 nm (2.79 eV), 467 nm (2.66 eV), and 502 nm (2.48 eV) were found to be the defect luminescence in Al_2O_3. The luminescence of F-centers in pure Al_2O_3 is at 440 nm (2.8 eV) [12,13], the luminescence of F2-centers is at 517 nm (2.4 eV) [14]. The F-centers and F2-centers lumine-scence band position were found to be close to the experimental result showing weak influence from the structure [15,16]. Thus, these defects might be present in $SrAl_2O_4$ and the F-centers, F2-centers could be responsible for luminescence peak at 445, 467 and 502 nm.

Long after glow (decay study): Fig. 10 shows the decay curve of pure $SrAl_2O_4$ phosphor. By curve fitting, the decay times of phosphor were calculated with the following exponential equation [17,18]:

$$I = I_o + k_1 \exp\left(-\frac{t}{\tau_1}\right) + k_2 \exp\left(-\frac{t}{\tau_2}\right) \quad (3)$$

where I represents the luminescence intensity after irradiating the sample, I_o, and k_1, k_2 are the constants; t is the time, τ is the decay constant. The decay parameters are significantly affected by the trap depths, deep traps are associated with long lifetimes, and shallow traps are associated with short lifetimes [18]. The decay constants based on the curve fitting with the equation are shown as an inset in Fig. 10. The average lifetime is found to be nearly 2 millisecond (ms).

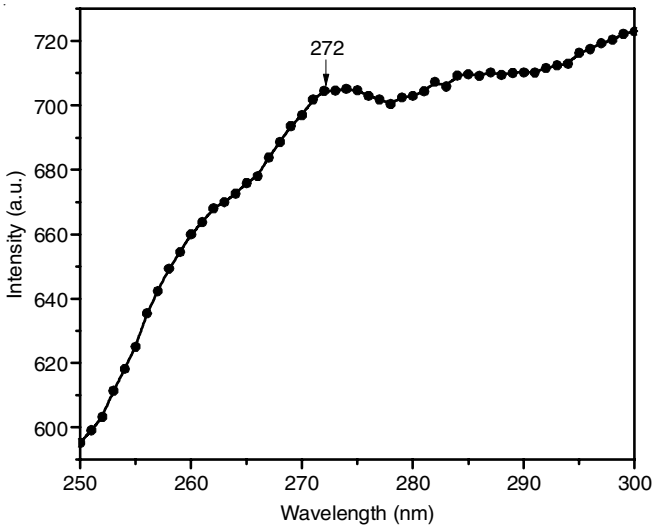

Fig. 9(a). Excitation spectrum of $SrAl_2O_4$ phosphor

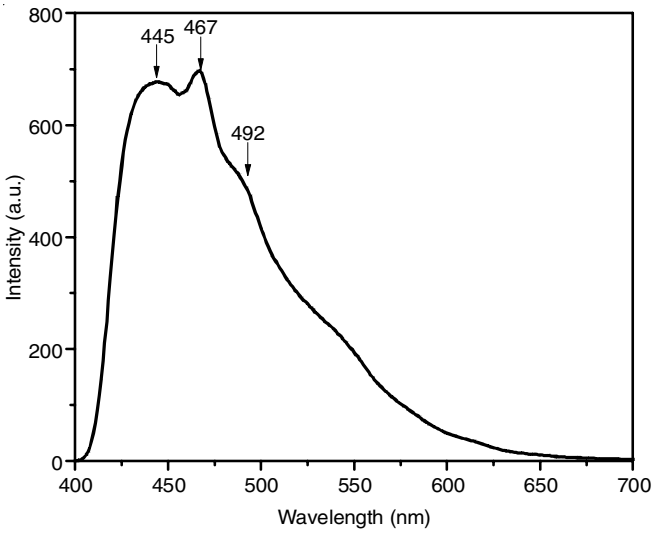

Fig. 9(b). Emission spectrum of $SrAl_2O_4$ phosphor

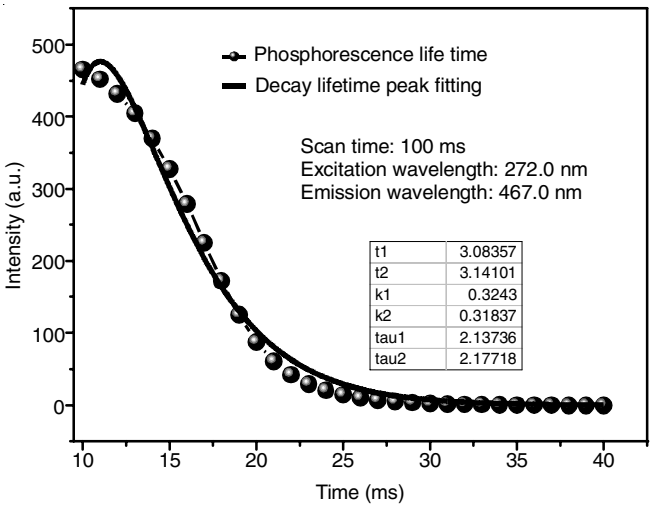

Fig. 10. Decay curve of $SrAl_2O_4$ phosphor

Electronic structure: The electronic structure calculation of $SrAl_2O_4$ phosphor is performed in the light of DFT using WIEN2k code developed by Blaha *et al*. [19]. Linearized augmented plane wave (LAPW) is used as the basis set, along with the generalized gradient approximation (GGA) as proposed by Perdew, Burke and Ernzerhof (PBE) as exchange-correlation potentials [20]. In this procedure, the lattice is divided into non-overlapping spheres called muffin tin (MT) sphere surrounding each atomic site and an interstitial region. Inside the muffin tin region, the basis function is a product of radial function and spherical harmonics. The basis functions are expanded in plane waves in the interstitial regions (outside muffin tin sphere). In the present calculations, 8000 k-points are used for the integration, and convergence of the basis set is obtained at $R_{MT}K_{max} = 9.0$ where K_{max} gives the plane wave cut-off and R_{MT} is the smallest atomic sphere radius in the unit cell. Initial crystal structure data used in the present work is taken from the Inorganic Crystal Structure Database (ICSD no. 26466). The purpose of DFT study is to create the energy band diagram as shown in Fig. 11. The calculated band gap from the band diagram is compared with the optical absorption experiment data. The band gap at the T point is found to be 4.4 eV, which is almost nearly equal to the value of 4.46 eV as determined from the optical absorption as discussed above.

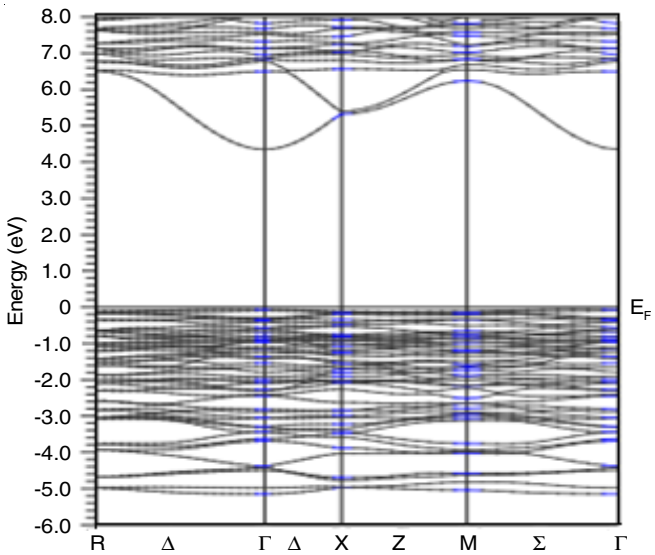

Fig. 11. Energy band diagram of $SrAl_2O_4$ phosphor

Conclusion

Pure $SrAl_2O_4$ phosphor is successfully prepared using the precipitation method and annealed at 1000 ºC. The prepared sample has been characterized. The XRD analysis of $SrAl_2O_4$ phosphor shows the monoclinic structure and requires heat treatment to obtain its monoclinic structure. The FTIR and EDX spectrum confirms the presence of constituent elements in the sample. Raman spectroscopy study revealed the presence of Al-O stretching vibrations, bending of O-Al-O bonds, Sr-O-Sr bonds. The TEM diffraction pattern shows the polymorphs are spherical shape without much agglomeration and the particles size are in the range of 5 to 112 nm. The photoluminescence emission spectrum shows a characteristic peak at 467 nm (blue) when excited at 272 nm wavelength. Theoretical calculation of energy band diagram using DFT shows the band gap of the $SrAl_2O_4$ phosphor is 4.4 eV, which is close to the band gap value of 4.46 eV obtained from the experimental results of the UV-visible absorption spectrum.

ACKNOWLEDGEMENTS

The authors thank IIT-Bombay, Mumbai for Raman analysis, and also Department of Chemistry, NIT Manipur, Imphal, India for its FTIR and PL measurements.

CONFLICT OF INTEREST

The authors declare that there is no conflict of interests regarding the publication of this article.

REFERENCES

1. T. Peng, L. Huajun, H. Yang and C. Yan, *Mater. Chem. Phys.*, **85**, 68 (2004); https://doi.org/10.1016/j.matchemphys.2003.12.001.
2. W. Hoogenstraaten and H.A. Klasens, *J. Electrochem. Soc.*, **100**, 366 (1953); https://doi.org/10.1149/1.2781134.
3. W.M. Yen, S. Shionoya and H. Yamamoto, Phosphor Handbook, CRC Press/Taylor and Francis: Boca Raton, edn 2 (2007).
4. T. Matsuzawa, Y. Aoki, N. Takeuchi and Y. Murayama, *J. Electrochem. Soc.*, **143**, 2670 (1996); https://doi.org/10.1149/1.1837067.
5. T. Katsumata, K. Sasajima, T. Nabae, S. Komuro and T. Morikawa, *J. Am. Ceram. Soc.*, **81**, 413 (1998); https://doi.org/10.1111/j.1151-2916.1998.tb02349.x.
6. K. Van den Eeckhout, P.F. Smet and D. Poelman, *Materials*, **3**, 2536 (2010); https://doi.org/10.3390/ma3042536.
7. D. Haranath, V. Shanker, H. Chander and P. Sharma, *J. Phys. D Appl. Phys.*, **36**, 2244 (2003); https://doi.org/10.1088/0022-3727/36/18/012.
8. T. Katsumata, T. Nabae, K. Sasajima, S. Komuro and T. Morikawa, *J. Elec. Soc.*, **144**, 243 (1997); https://doi.org/10.1149/1.1837931.
9. I.V. Kityk, J. Wasylak, D. Dorosz and J. Kucharski, *Opt. Laser Technol.*, **33**, 157 (2001); https://doi.org/10.1016/S0030-3992(01)00012-3.
10. M. Ayvacikli, Z. Kotan, E. Ekdal, Y. Karabulut, A. Canimoglu, J. Garcia Guinea, A. Khatab, M. Henini and N. Can, *J. Lumin.*, **144**, 128 (2013); https://doi.org/10.1016/j.jlumin.2013.06.040.
11. Z. Tang, F. Zhang, Z. Zhang, C. Huang and Y. Lin, *J. Eur. Ceram. Soc.*, **20**, 2129 (2000); https://doi.org/10.1016/S0955-2219(00)00092-3.
12. E. Finley, A.S. Paterson, A. Cobb, R.C. Willson and J. Brgoch, *Opt. Mater. Express*, **7**, 2597 (2017); https://doi.org/10.1364/OME.7.002597.
13. E. Shafia, A. Aghaei, M. Bodaghi and M. Tahriri, *J. Mater. Sci. Mater. Electron.*, **22**, 1136 (2011); https://doi.org/10.1007/s10854-010-0273-x.
14. C. Chang, Z. Yuan and D. Mao, *J. Alloys Compd.*, **415**, 220 (2006); https://doi.org/10.1016/j.jallcom.2005.04.219.
15. B. Cheng, Z. Zhang, Z. Han, Y. Xiao and S. Lei, *CrystEngComm*, **13**, 3545 (2011); https://doi.org/10.1039/c0ce00934b.
16. M. Ayvacikli, A. Ege, S. Yerci and N. Can, *J. Lumin.*, **131**, 2432 (2011); https://doi.org/10.1016/j.jlumin.2011.05.051.
17. D.S. Kshatri, A. Khare and P. Jha, *Optik*, **124**, 2974 (2013); https://doi.org/10.1016/j.ijleo.2012.09.045.
18. K. Hadjiivanov, A. Davydov and D. Klissurski, *Kinet. Catal.*, **29**, 161 (1988).
19. P. Blaha, K. Schwarz, G.K.H. Madsen, D. Kvasnicka and J. Luitz, WIEN2k-An Augmented Plane Wave Plus Local Orbitals Program For Calculating Crystal Properties, User's Guide, WIEN2k_19.1 (2019).
20. J. Perdew, K. Burke and M. Ernzerhof, *Phys. Rev. Lett.*, **77**, 3865 (1996); https://doi.org/10.1103/PhysRevLett.77.3865.